

# Stepped Silicon Surfaces as Templates for One-Dimensional Nanostructures<sup>†</sup>

F. J. Himpsel,<sup>\*,‡</sup> J. L. McChesney,<sup>‡</sup> J. N. Crain,<sup>‡</sup> A. Kirakosian,<sup>‡</sup> V. Pérez-Dieste,<sup>‡</sup> Nicholas L. Abbott,<sup>§</sup> Yan-Yeung Luk,<sup>§</sup> Paul F. Nealey,<sup>§</sup> and Dmitri Y. Petrovykh<sup>||</sup>

Department of Physics, University of Wisconsin-Madison, Madison, Wisconsin 53706, Department of Chemical and Biological Engineering, UW-Madison, Madison, Wisconsin 53706, Physics Department, University of Maryland, College Park, Maryland 20742, and Naval Research Laboratory, Washington, D.C. 20375

Received: February 20, 2004

It is shown how atomically precise step arrays can be fabricated on vicinal Si(111). Decoration with metal atoms produces atomic chains that serve as the ultimate nanowires for the study of electrons between one and two dimensions. Chain structures are formed by a large variety of metal atoms with different chemical properties. They range from alkali and alkaline earth metals to noble metals and include transition metals (Pt) and rare earths (Gd, Ho). As a first step toward functionalizing such surfaces, we demonstrate how NEXAFS spectroscopy characterizes organic layers in atom- and orbital-specific fashion, with examples ranging from alkanes with customized end groups to DNA oligonucleotides.

## 1. Motivation and Outline

Since the early years of surface science, it has been recognized that well-defined single-crystal surfaces offer an opportunity to reveal the fundamental mechanisms behind complex phenomena, such as thin-film growth and heterogeneous catalysis.<sup>1</sup> After several decades of ever-increasing sophistication in the preparation of single-crystal surfaces, it is now feasible to tailor them in many ways. For example, atomically precise arrays of steps and kinks can be produced at vicinal surfaces.<sup>2–9</sup> These may serve as templates for the growth of low-dimensional structures<sup>10–12</sup> and as prototypes for reactive sites in supported catalysts. Chains of metal atoms can be assembled on these structures using a large variety of metals, from alkalis and alkaline earths to gold, platinum, and rare earths.<sup>2,13–22</sup> Many of these chain structures are metallic and thus represent the finest possible nanowires.

After assembling one-dimensional arrays of atoms on silicon, one can proceed to use them as templates for creating prototype electronic devices. An example is a toy memory where a bit is stored by the presence or absence of a single silicon atom.<sup>23,24</sup> Such a structure serves as a testbed for exploring fundamental limits of storage density and readout speed, showing that these two quantities are complementary and thus require a tradeoff.

The challenge is now to go beyond simple self-assembly of repetitive structures and to build up a more complex architecture from self-assembled components, for example, by combining magnetic nanocrystals<sup>25,26</sup> with a silicon template into a patterned storage medium where a single nanocrystal stores one bit. This would be a more evolutionary development of present hard disk technology. Even though hard disks have the highest areal density of the storage devices in use today, they still need a few hundred magnetic grains to store one bit. For assembling complex structures, it is natural to enlist physical chemistry with

its diverse repertoire of interactions, including hydrophilic/hydrophobic interactions between organic molecules.

A long-term goal is the ordered assembly of small proteins and artificial membranes at surfaces. That provides a controllable environment for unraveling the incredibly complex biological machinery.<sup>27</sup> Such a plan is analogous to the original concept of understanding heterogeneous catalysis via chemisorption at well-defined surfaces. Initially, one will have to solve the problem of appropriately attaching biological molecules and structures in a controllable way that preserves their functionality. For example, an Australian group<sup>28</sup> has embarked on a program of assembling a phospholipid membrane supported by molecular stilts above a surface, where separate liquids can be introduced underneath and above the membrane to simulate the outside and inside of a cell. These simple artificial membranes then can be further functionalized by incorporation of biological molecular machinery, such as channel proteins or photosynthesis centers.

In the following, we present recent progress along the early stages of such a program. We begin with stepped silicon templates, add chains of metal atoms, and let them self-assemble into an atomic scale memory. Eventually, the attachment and characterization of organic molecules all the way up to DNA oligonucleotides is explored. Near-edge X-ray absorption fine structure (NEXAFS) spectroscopy is an incisive tool for determining coverage and orientation of organic layers.<sup>26,29–33</sup> It is possible to single out specific regions of an organic molecule by selecting particular atoms via their core levels and oxidation states and connecting them with specific molecular orbitals in an optical transition.

## 2. Stepped Si(111) Templates

Figure 1 gives an overview of the types of step arrays that can be produced on vicinal Si(111) surfaces by self-assembly.<sup>2–7</sup> Large features in the 80-nm range can be obtained by tilting the surface normal toward the  $[11\bar{2}]$  azimuth where step bunching is observed. This length scale connects with the smallest features obtained by standard optical lithography today. An opposite tilt toward the  $[1\bar{1}2]$  azimuth creates steps that are

<sup>†</sup> Part of the special issue "Gerhard Ertl Festschrift".

<sup>\*</sup> Corresponding author. E-mail: fhimpsel@facstaff.wisc.edu.

<sup>‡</sup> Department of Physics, UW-Madison.

<sup>§</sup> Department of Chemical and Biological Engineering, UW-Madison.

<sup>||</sup> University of Maryland and Naval Research Laboratory.

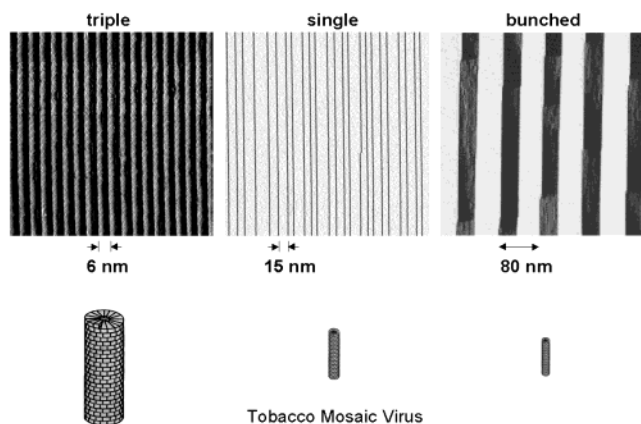


**Figure 1.** Step arrays obtained by self-assembly on vicinal Si(111) surfaces.<sup>4–6</sup> The largest step period of 80 nm (right) makes a connection with standard lithography, the intermediate period of 15 nm is comparable to the size of a virus, and the smallest period of 6 nm (17 atom rows) matches the size of a protein molecule. The steps can be made very straight (e.g., only one kink in 20 000 edge atoms in the center panel) since the large  $7 \times 7$  unit cell requires the addition of many atomic rows at a kink site. Step periods below 6 nm can be controlled with atomic precision via the increasing step–step interaction. These and all following STM images are derivatives of the topography in the  $x$ -direction, which emphasizes steps as dark lines.

one-double-layer high with a typical spacing of 15 nm at a  $1^\circ$  tilt angle. Looking ahead to the potential of such structures for assembling biological objects, it is interesting to note that these dimensions are comparable to that of a typical virus, such as the rodlike tobacco mosaic virus. Going to even higher tilt angles of the order  $10^0$ , one can produce step arrays with a spacing of about 6 nm. These features are comparable to the wedge-shaped protein molecules that make up the cylindrical shell of the tobacco mosaic virus.

Although chain structures can be found on other semiconductor surfaces, such as Si(100) and GaAs(110), there is a substantial benefit in choosing the Si(111) $7 \times 7$  surface with its large unit cell. The native defect of a step is a kink, and it becomes difficult to create kinks for surfaces with a large unit cell. For example, the double-layer structure of the Si(111) $7 \times 7$  surface requires the addition of  $2 \cdot 7 = 14$  rows at a kink site. Kink densities as low as 1 in 20 000 edge atoms have been achieved<sup>4</sup> (Figure 1 center). A similar effect has been observed for stepped metal surfaces with a large unit cell, such as Au(111).<sup>8</sup> Semiconductor surfaces are particularly interesting for studies of low-dimensional electrons because surface states inside the gap cannot couple to the substrate.

While steps can be made extremely straight on Si(111) $7 \times 7$ , their spacing is more difficult to control. One has to reduce the step spacing to about 6 nm until the step–step interaction becomes large enough to force a regular spacing (Figure 1 left). The Si(557) $3 \times 1$  surface shown here is particularly stable.<sup>6,7</sup> It contains exactly 17 atom rows per period in the [111] projection and can thus be used as a highly precise ruler for metrology at the nanometer scale. The period is tied directly to the Si lattice constant, which is a secondary length standard. The tripling of the step height provides a further boost to the step–step interaction in this case. The terrace contains a single  $7 \times 7$  cell, thus representing the narrowest structure that is able to sustain the  $7 \times 7$  reconstruction. The step corresponds to a Si(113) facet,<sup>7</sup> which is one of the most stable silicon facets. In general, one can say that the self-assembly process becomes atomically precise as one approaches atomic dimensions,

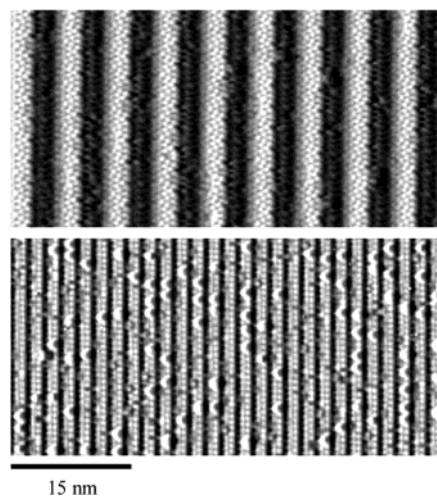


**Figure 2.** Creating atomic chains by depositing one-fifth of a monolayer of Au onto the Si(557) surface.<sup>6,16</sup> The clean surface has a triple-step structure containing a single  $7 \times 7$  unit cell (top). It is converted into a single-step structure with atomic chains (bottom).

because the energy difference between structures differing by one atom row becomes significant.

### 3. Atomic Chains

The next step in the construction of one-dimensional arrays is the decoration of step structures with extra atoms. Metal atoms are particularly interesting since metallic surfaces have rather diverse phase diagrams which include low-dimensional instabilities, such as charge density waves, spin density waves, and exotic forms of superconductivity. Figure 2 shows how the triple-step structure of Si(557) $3 \times 1$  is converted to a single-step structure after deposition of one-fifth of a monolayer of Au. Atomic chains can now be seen in the STM image. One might expect that the Au atoms decorate the step edges where they find higher coordination. This concept is turned on its head by nature, like so many other simple-minded predictions in nanoscience. The Au atoms actually form a chain at the center of the terrace, not at the step edge, according to local density theory<sup>18,21</sup> and X-ray diffraction.<sup>17</sup> They are incorporated into the surface substituting Si atoms in the first layer. As a consequence, the chains seen in the STM image are not the Au atoms that were deposited, but silicon atoms with broken bonds. Local density calculations<sup>18</sup> show that the Au atoms grab an electron from nearby Si atoms and pair it with the Au  $s,p$ -electron to form a fully occupied band well below  $E_F$ . This scenario makes sense, since Au is more electronegative than Si.

Chain structures can be obtained with a variety of metal atoms, such as alkalis, alkaline earths, noble metals (Ag, Au), transition metals (Pt), and rare earths (Gd, Ho). Figure 3 shows a recently discovered chain structure induced by Pt, which brings catalytically active  $d$ -electrons into play. This structure combines two periods (see the center and bottom of Figure 3). The fundamental chain period corresponds to a Si(337) structure, which consists of three Si(111) and two Si(100) unit cells. After four of these Si(337) unit cells, a small slip occurs in the sequence of Si(111) and Si(100) facets. A Si(111) facet is shortened from three to two rows. The resulting superlattice of chains corresponds to the Si(11 11 27) orientation. It has a period of 5.99 nm, which approaches the upper limit for the arrays that self-organize with atomic precision (compare the Si(557) $3 \times 1$  surface with 5.73-nm period and the Si(5 5 12) $2 \times 1$  surface with 5.35-nm period<sup>8</sup>).

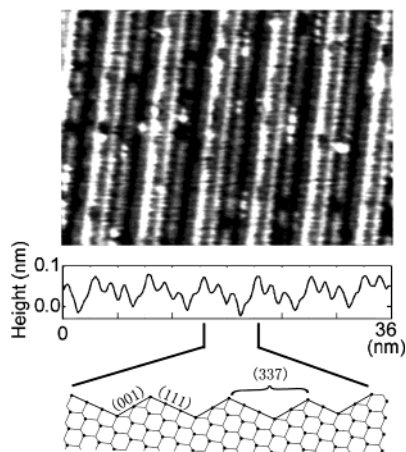


**Figure 3.** Chain structure induced by Pt on stepped Si(111), the first of this kind containing d-electrons. It exhibits two periods, a fundamental period of 1.6 nm corresponding to the Si(337) lattice, and a superlattice induced by a phase slip every four unit cells, corresponding to Si(11 11 27) with an overall period of 6 nm.

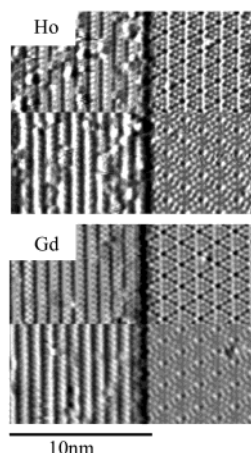


**Figure 4.** Chain structures of two rare earths induced on Si(111). Both Gd and Ho form similar structures, where chains of occupied and empty orbitals alternate (for Gd see ref 22). This is evidenced by a displacement of the chains between the top and bottom half of each image, where the sample bias changes sign (occupied states in the bottom half and empty states in the top half of each image, using  $\pm 1.2$  V bias for Gd and  $\pm 2$  V for Ho). A patch of clean Si(111)  $7 \times 7$  on the right does not exhibit such a displacement.

Chain structures created by rare earths are shown in Figure 4 for Gd<sup>22</sup> and Ho. Rare earths introduce f-electrons with large magnetic moments and thus become prototypes for spin chains. Both Gd and Ho exhibit a  $5 \times 2$  chain structure on Si(111), which contains a peculiar arrangement of chains with filled and empty orbitals. These can be viewed as an array of lines with alternating charges. The observation that rare earths have a tendency to form similar structures makes it possible to vary the magnitude of the spins systematically by the f-count while keeping structural and charge characteristics the same.

Not all chain structures are metallic, but most of the Au-induced chains are. We have found them on a rich variety of vicinal Si(111) surfaces including all surfaces with odd Miller indices that we have studied. This includes surfaces tilted toward  $[1\bar{1}2]$  with nominally two broken bonds at the step edge, such as (335), (337), and (557), as well as surfaces tilted toward  $[1\bar{1}\bar{2}]$  with one broken bond at the edge, such as (110), (553), (775), (995), and (13 13 7). Even the flat Si(111) surface breaks its threefold symmetry at a coverage of two-fifths of a monolayer of Au and forms a Si(111)  $5 \times 2$ -Au chain structure. By going

to shallower tilt angle, the spacing between the chains increases, which makes it possible to systematically decrease the two-dimensional coupling between the chains and to approach the one-dimensional limit.

With so many chain structures forming on vicinal Si(111) surfaces, and even on flat Si(111), it is natural to ask whether there is a common structural feature that stabilizes the chains. In fact, total energy calculations for chain structures induced by alkalis, alkaline earths, and noble metals suggest a common feature, the honeycomb chain.<sup>13,18,21</sup> A graphitic stripe of Si atoms covers a bulklike Si(111) surface and forms one of the most stable configurations for the Si(111) surface. The stripe can be extremely long (hundreds of nanometers), but it is less than two hexagons wide. This suggests nearly perfect lattice match along the stripe (in the  $[1\bar{1}0]$  direction), but a very poor match perpendicular to it (in the  $[\bar{1}\bar{1}2]$  direction). Although absent in bulk Si,  $\pi$ -bonding is not unusual at silicon surfaces. It occurs in the  $\pi$ -bonded chain of the Si(111)  $2 \times 1$  cleavage surface and in the  $\pi$ -bonded dimers of Si(100)  $2 \times 1$ .

#### 4. Electrons between One and Two Dimensions

Physics is particularly simple and elegant in one dimension. Problems can often be solved analytically in one dimension but not in higher dimensions. Some problems involving highly correlated electrons can only be solved at all in one dimension. While theorists have it easier in one dimension, experimentalists encounter great difficulties in creating truly one-dimensional structures. An infinite chain of atoms freely suspended in space is simply not feasible. Even if it could be assembled, such a chain would not be very rigid. Atom chains have been achieved in a vacuum (between an STM tip and a surface), but they are only a few atoms long. Nature gives us a rather limited repertoire of quasi-one-dimensional systems, such as three-dimensional crystals consisting of transition-metal chains spaced by ionic groups or stacks of organic molecules with overlapping  $\pi$ -systems, such as the Bechgaard salts.<sup>34</sup> These systems leave little room for systematically varying the parameters that determine a one-dimensional phase diagram and they always exhibit a residual three-dimensional coupling that dominates the ground state at low temperatures.

Atomic chains at a semiconductor or insulator surface have several appealing properties for exploring the electronic structure of one-dimensional systems. While the chain atoms are firmly locked to the substrate lattice, the electrons near the Fermi level  $E_F$  are completely decoupled from the substrate. These states are located in the band gap of the substrate and have no bulk states to hybridize with. Of course, there are lower-lying states for the back-bonds that hold the chain atoms to the surface and interact strongly with the substrate. Unlike the electrons at  $E_F$ , the low-lying states are not relevant for the electronic properties, such as transport, magnetism, superconductivity, and charge density waves. While the chain states near  $E_F$  lack three-dimensional coupling, they still are coupled in two dimensions via chain–chain interactions. Such coupling can be reduced systematically by increasing the chain spacing via a shallower tilt angle of the surface from a low index plane, such as Si(111). We have been able to vary the 1D/2D coupling ratio from 12:1 to  $>100:1$  in this fashion,<sup>21</sup> while natural compounds, such as the Bechgaard salts, are limited to a ratio with substantial two-dimensional coupling (about 10:1).<sup>34</sup>

The 1D/2D coupling ratio is measured by mapping the band structure of the chains with angle-resolved photoemission.<sup>20,21</sup> There are two types of measurements leading to similar

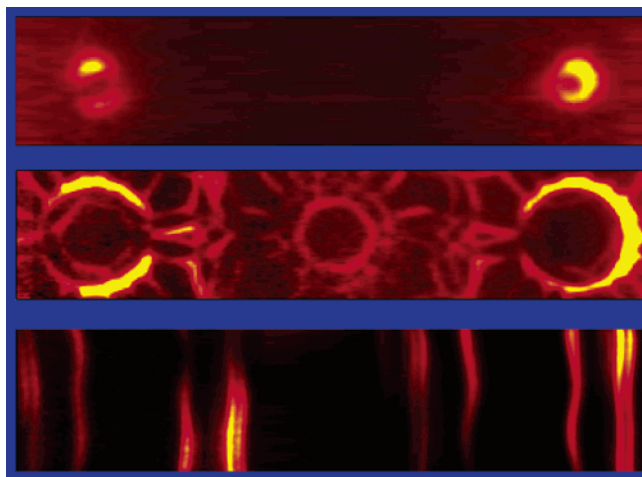


**Figure 5.** Fermi surfaces of two- and one-dimensional structures formed by silver and gold on silicon surfaces.<sup>20,35</sup> Circles are seen for two-dimensional structures, and lines for one-dimensional chains. The top panel shows small circles for the Fermi surface of the  $\text{Si}(111)\sqrt{3} \times \sqrt{3}$ -Ag surface doped by 1% of a monolayer of excess Ag. The middle panel is for a  $\sqrt{21} \times \sqrt{21}$  superlattice built up on top of the  $\text{Si}(111)\sqrt{3} \times \sqrt{3}$ -Ag superlattice by adding 0.2 monolayer of Au. The Fermi circles are larger because of the higher band filling, and replicas appear because of diffraction at the  $\sqrt{21} \times \sqrt{21}$  superlattice. The bottom panel for the  $\text{Si}(553)$ -Au chain structure shows one-dimensional Fermi lines with small undulations representing residual coupling between the chains. The momentum parallel to the chains is plotted horizontal.

results: The energy-versus-momentum band dispersion can be measured parallel and perpendicular to the chains. The ratio of the bandwidths provides the coupling ratio. The most striking differences between two- and one-dimensional bands appear at the Fermi surface, where the electronic states at  $E_F$  are displayed as a function of the in-plane momentum (Figure 5). Two-dimensional Fermi surfaces are characterized by closed curves, such as the Fermi circles observed for the  $\text{Si}(111)\sqrt{3} \times \sqrt{3}$ -Ag and  $\text{Si}(111)\sqrt{21} \times \sqrt{21}$ -(Ag + Au) structures.<sup>35</sup> These are obtained at noble metal coverages of a monolayer and higher. A truly one-dimensional Fermi surface consists of two points at  $\pm k_F$ , but these become straight lines when plotted in two dimensions. The energy is independent of the momentum perpendicular to the chains (vertical in Figure 5). An actual chain structure, such as  $\text{Si}(553)3 \times 1$ -Au, displays undulating lines. The amplitude of the undulations is a measure of the residual two-dimensional coupling. The complete set of data can be reproduced by a tight binding calculation that includes two couplings along the chains ( $t_1$  and  $t_3$  for first and second neighbor) and one between the chains ( $t_2$ ). The dimensionality ratio is given by  $t_1/t_2$ . For this particular structure, one observes a doublet of closely spaced Fermi lines with  $t_1/t_2 = 39, 46$  and a single line with  $t_1/t_2 = 12$ .

In addition to the coupling, it is possible to vary the band filling of these Au chain structures. The two closely spaced bands in Figure 5 are slightly more than half-filled, and the single band is one-fourth filled, bringing the total filling to exactly four-thirds (within the accuracy of the measurement of  $\pm 1.5\%$ ). The fractional filling brings up interesting questions about a possible analogue to the fractional quantum Hall effect in 1D. It is not obvious how two-dimensional Landau orbits will be transformed by an array of loosely coupled one-dimensional chains. Seeing two-half-filled bands raises another intriguing question: Why does the surface choose two-half-filled bands, corresponding to two broken bonds, instead of one completely filled band? The answer is still open, showing that

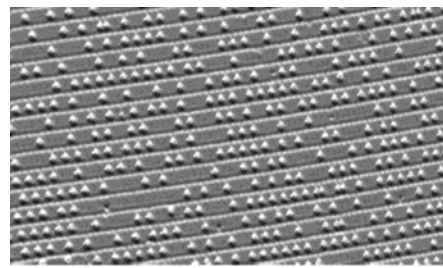


**Figure 6.** The  $\text{Si}(111)5 \times 2$ -Au structure serving as atomic scale memory, where the presence or absence of a single Si atom represents one bit.<sup>23</sup> The underlying chain structure provides atomically precise tracks with a pitch of five atom rows (1.66 nm). The memory is preformatted by ones by depositing Si on all possible  $5 \times 4$  lattice sites. A zero is written by removing one of the Si atoms with the tip of a scanning tunneling microscope.

the exotic electronic properties of these chain structures remain full of interesting challenges.

## 5. Atomic Scale Memory

One of the first applications of atomic chain structures is a memory at the atomic limits of data storage.<sup>23</sup> The  $\text{Si}(111)5 \times 2$ -Au structure provides atomically precise tracks with a pitch of five atom rows (1.66 nm), as shown in Figure 6. Extra silicon atoms on top of the chains store the bits. A one (zero) is stored by the presence (absence) of a single silicon atom inside a  $5 \times 4$  cell. The memory is preformatted with ones by depositing Si atoms onto all sites, and the zeros are written by removing the Si atoms with the tip of a scanning tunneling microscope. This memory operates at room temperature. More sophisticated versions of an atomic memory can be realized at liquid helium temperature, where atom manipulation is much easier. Atoms can be chosen that have a 50 times lower diffusion barrier and thus require little force to be moved. In the room-temperature memory, the extra Si atoms have a diffusion barrier of 1.2 eV, which gives them a hopping rate of about 1 in every 2–3 years.<sup>23</sup>

An atomic memory can be used to address some basic questions about data storage in general: What is the highest possible data storage density and the maximum data rate? How does this compare to information storage in DNA? When can I buy such a memory? The density limit is determined by the interactions between adjacent bits. The bit-to-bit correlation can be used to quantify the potential acting between the extra Si atoms.<sup>24</sup> We find that for this particular structure, the  $5 \times 4$  bit cell is the smallest possible, because the repulsion between atoms in adjacent  $5 \times 2$  unit cells is too large, that is, changing a bit in a  $5 \times 2$  cell without affecting the atom in the next  $5 \times 2$  cell would not be possible. The  $5 \times 4$  limit is remarkably close to Feynman's 1959 estimate of  $5 \times 5 \times 5$  atoms per bit in a three-dimensional memory. Regarding the data rate, we predict a leveling-off and eventual slowdown with increasing storage density. The readout signal per bit becomes weaker and requires longer integration times to preserve the signal/noise ratio. The density and data rate for this memory are both close to those of DNA, while the density is more than 3 orders of magnitude higher than in hard disks and the data rate 6 orders of magnitude lower.

The signal/noise ratio is limited by statistical noise, not by thermal noise, because the electrons tunnel from a resonance of the Si atoms at 2 eV below  $E_F$ , an energy much larger than  $k_B T = 25$  meV. With an ideal amplifier and feedback system, one could achieve the same signal/noise with a  $10^5$  time higher data rate, but that is still an order of magnitude slower than

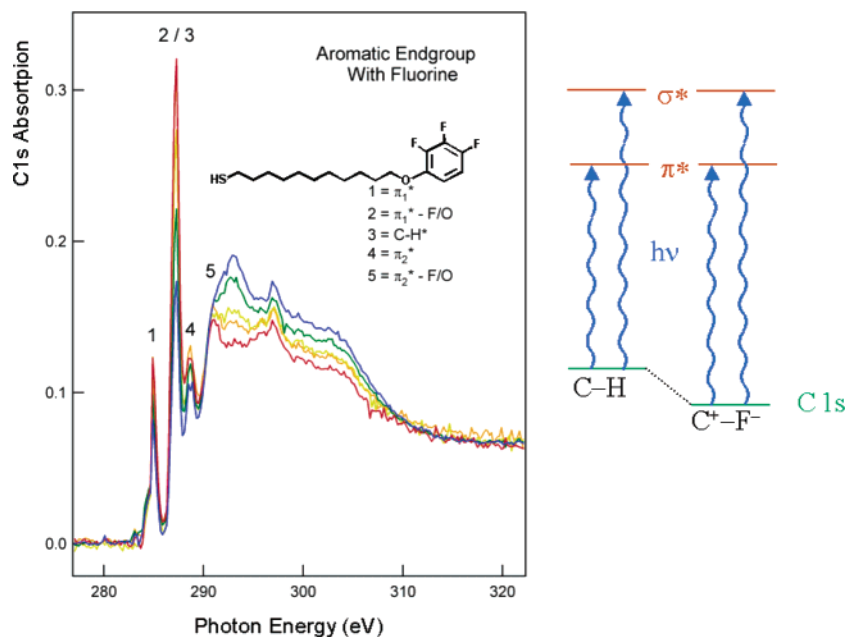


**Figure 7.** Probing the electronic structure of self-assembled monolayers of alkane chains with aromatic end groups.<sup>31</sup> Transitions from a core level to the lowest unoccupied orbitals are observed by NEXAFS. Specific atoms can be addressed by selecting a particular absorption edge (here C 1s) and by using the chemical shift of the core level (here C–H versus C<sup>+</sup>–F<sup>–</sup>). Specific orbitals in the final state can be addressed as well, such as  $\pi^*$  and  $\sigma^*$ .

today's hard disks. Only a highly parallel architecture can offset this fundamental slowdown, such as a large array of sensors. The question about commercial availability can at best be addressed by using Moore's law for Si technology. If one extrapolates the areal density of Si DRAM to the density of 250 Terabit/inch<sup>2</sup> for the atomic scale memory, one obtains the year 2038 for commercial availability.

Although this memory might be considered as the ultimate in storage density, the writing process is extremely slow and unreliable because it involves removing atoms with the tip of a scanning tunneling microscope. Currently, we are working on replacing atoms by molecules, which can be switched electrically by the STM tip. For example, one could try using the tip voltage to rotate polar molecules<sup>36</sup> or flip bistable molecules.<sup>37</sup> A whole field of molecular electronics is developing around switchable molecules and has already led to a prototype memory developed at Hewlett-Packard. These devices use thousands of molecules per bit. For constructing a memory with a single molecule per bit, it will be critical to find ways for attaching molecules to a chain structure in specific locations such that they form a regularly spaced sequence similar to that of the extra Si atoms on the Si(111)5 × 2 chains. Specific adsorption of hydrocarbons has been achieved at flat semiconductor surfaces,<sup>38,39</sup> and one-dimensional arrays of molecules have been attached to anisotropic metal surfaces.<sup>38,39</sup> This knowledge needs to be transferred to silicon chain structures and adapted to their high chemical reactivity and complex atomic arrangement.

## 6. Functionalization and Characterization by NEXAFS

After producing one-dimensional structures on silicon surfaces by self-assembly, one can use them as stepping stones for the assembly of more complex structures that have some type of functionality, such as a biosensor or a data storage medium. Such attempts are still in early stages as far as nanostructured silicon surfaces are concerned, but there has been substantial progress already on simpler surfaces, such as gold-covered glass.<sup>27,28</sup> For reaching a control of the self-assembly process with a precision that matches atomically precise silicon sub-

strates, it is essential to have techniques that characterize the growing layers, their coverage, structure, orientation, and their chemical bonding.

An incisive technique for characterizing organic layers all the way up to macromolecules is NEXAFS (near-edge X-ray absorption fine structure spectroscopy).<sup>29</sup> This technique measures transitions from core levels to empty valence orbitals, as illustrated in Figure 7, by applying it to a self-assembled monolayer containing an alkane backbone and an aromatic end group.<sup>31</sup> NEXAFS is sensitive to the identity of an atom (C, N, F,...) and to its charge state via the chemical shift (as in XPS). In addition, a specific orbital can be identified at that atomic location, such as a  $\pi^*$  or  $\sigma^*$ , a C–H or a C–C bond. This is shown in Figure 7, where the peaks in the spectrum can be assigned to specific atoms and orbitals.<sup>31</sup> The end group can be separated from the alkane backbone, and even specific parts of the end group can be identified, such as C atoms in the phenyl ring bonding to H versus F. Furthermore, polarization selection rules make it possible to determine the orientation of any of these orbitals, as shown in Figure 8.

Figure 8 demonstrates how sensitive the functionalization of silicon surfaces is to the exact preparation conditions. In this case, OTS (octadecyltrichlorosilane) was applied in a humid and a dry environment,<sup>30</sup> giving rise to an oriented layer with strong polarization dependence in the first case (left) and to a random layer in the second (right). In addition, one can see directly from the intensity increase (1.5 units versus 0.5 units relative to the pre-edge signal) that the ordered layer is 3 times denser than the disordered layer. OTS forms a self-assembled monolayer (SAM) on oxidized surfaces (silicon, glass), as an alternative to the thiol chemistry, which operates on noble metal surfaces. Such SAMs can be used to attach biomolecules to surfaces.<sup>27</sup>

This type of analysis can be carried over to more complex molecules, such as DNA oligonucleotides<sup>32,33</sup> and even small proteins. DNA lends itself to highly selective spectroscopy by NEXAFS, because the bases are the only part of the molecule containing nitrogen. Furthermore, these nitrogens are incorpo-

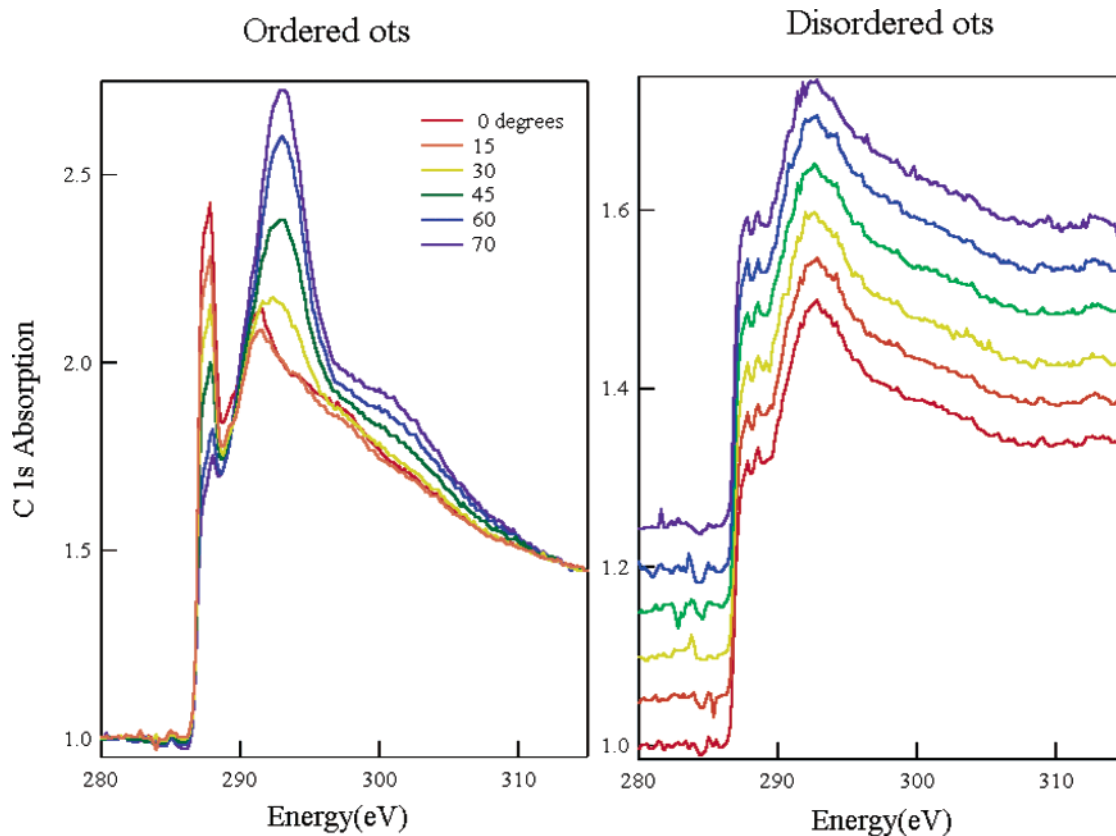


**Figure 8.** Functionalization of an oxide surface via siloxane chemistry.<sup>30</sup> The coverage can be probed by the height of the C 1s edge jump and the orientation of the alkane chains by the polarization dependence. Both depend strongly on the preparation, with a dry environment leading to a less dense, completely disordered layer.

rated into  $\pi$ -bonded ring systems, which provide sharp  $\pi^*$  orbitals as final states for the N 1s core electron. Our initial experiments<sup>32</sup> demonstrate that the N atoms in the base pairs can be selectively detected by NEXAFS, although the signal is only about 3% of the background. A signal/noise ratio of  $10^{-4}$  is required for reliable measurements when detecting electrons as decay products of the core hole created in NEXAFS. Nevertheless, clear orientation effects can be observed. In a DNA double-helix, all the N  $\pi^*$  orbitals point along the axis of the double helix, making it possible to infer the orientation of the molecule from the polarization dependence of the N 1s to  $\pi^*$  transitions.

The poor signal/background ratio of dilute species, such as the nitrogen in DNA, can be vastly improved by using NEXAFS with fluorescence detection instead of the usual total electron yield detection.<sup>26</sup> Instead of collecting secondary electrons from all core levels, one can filter out the fluorescence from a specific element. The fluorescence cross section is only a small fraction of the Auger and secondary electron cross section for the primary elements of organic chemistry (about  $10^{-4}$ – $10^{-5}$ ). Third generation synchrotron light sources make up for the low efficiency, and radiation damage can be held in check by illuminating a large area and collecting a substantial solid angle with a channel plate plus a filter. Recently, we have been able to systematically study the changes in the orientation of DNA oligonucleotides with different preparation methods by using this method.<sup>33</sup>

In the future, the combination of several highly specific detection methods will be crucial for getting the assembly of complex organic molecules under control, for example, combining NEXAFS for electronic states with FTIR for characteristic vibrations. Using NEXAFS with fluorescence detection,

one is able to take advantage of its large probing depth (about 100 nm for photons versus 2 nm for electrons at energies of a few 100 eV). Looking deeper into organic and biomaterials reduces the disturbance by the vacuum environment. In fact, it is possible to operate NEXAFS in an equilibrium background pressure of water vapor by using silicon nitride membranes to confine the water vapor. Even thin liquid water cells with silicon nitride windows have been fabricated. Thus, one can expect that NEXAFS will remain a useful technique when our rather primitive attempts have evolved into a more realistic rendering of artificial biosystems, which will have to operate in aqueous environment. One might even consider tracking the dynamics of such systems in real time. Fascinating nonequilibrium phenomena have been observed during pattern formation in surface chemical reactions.<sup>42</sup> It is likely that biochemical reactions with their strong feedback exhibit them, too.

**Acknowledgment.** This work was supported by the NSF under Award No. DMR-0240937 and DMR-0079983, and by the DOE under Contract No. DE-FG02-01ER45917. It was conducted at the SRC (NSF Award No. DMR-0084402) and at the ALS (DOE Contract No. DE-AC03-76SF00098).

## References and Notes

- (1) Ertl, G. *Surf. Sci.* **1994**, 299/300, 742.
- (2) Petrovykh, D. Y.; Himpel, F. J. Self-assembled nanostructures at silicon surfaces. In *Encyclopedia of Nanoscience and Nanotechnology*; Nalwa, H. S., Ed.; American Scientific Publishers: in press, 2004.
- (3) Williams, E. D.; Bartelt, N. C. *Science* **1991**, 251, 393.
- (4) Viernow, J.; Lin, J.-L.; Petrovykh, D. Y.; Leible, F. M.; Men, F. K.; Himpel, F. J. *J. Appl. Phys. Lett.* **1998**, 72, 948.
- (5) Lin, J.-L.; Petrovykh, D. Y.; Viernow, J.; Men, F. K.; Seo, D. J.; Himpel, F. J. *J. Appl. Phys.* **1998**, 84, 255.

- (6) Kirakosian, A.; Bennewitz, R.; Crain, J. N.; Fauster, Th.; Lin, J.-L.; Petrovykh, D. Y.; Himpfel, F. J. *Appl. Phys. Lett.* **2001**, *79*, 1608.
- (7) Henzler, M.; Zhachuk, R. *Thin Solid Films* **2003**, *428*, 129.
- (8) Baski, A.; Erwin, S. C.; Whitman, L. J. *Science* **1995**, *169*, 1556.
- (9) Repain, V.; Berroir, J. M.; Croset, B.; Rousset, S.; Garreau, Y.; Etgens, V. H.; Lecoœur, L. *Phys. Rev. Lett.* **2000**, *84*, 5367.
- (10) Viernow, J.; Petrovykh, D. Y.; Men, F. K.; Kirakosian, A.; Lin, J.-L.; Himpfel, F. J. *Appl. Phys. Lett.* **1999**, *74*, 2125.
- (11) Rauscher, H.; Jung, T. A.; Lin, J.-L.; Kirakosian, A.; Himpfel, F. J.; Rohr, U.; Müllen, K. *Chem. Phys. Lett.* **1999**, *303*, 363.
- (12) Gambardella, P.; Blanc, M.; Brune, H.; Kuhnke, K.; Kern, K. *Phys. Rev. B* **2000**, *61*, 2254.
- (13) Erwin, S. C.; Weitering, H. H. *Phys. Rev. Lett.* **1998**, *81*, 2296.
- (14) Jalochoowski, M.; Stozak, M.; Zdyb, R. *Surf. Sci.* **1997**, *375*, 203.
- (15) Segovia, P.; Purdie, D.; Hengsberger, M.; Baer, Y. *Nature* **1999**, *402*, 504.
- (16) Losio, R.; Altmann, K. N.; Kirakosian, A.; Lin, J.-L.; Petrovykh, D. Y.; Himpfel, F. J. *Phys. Rev. Lett.* **2001**, *86*, 4632.
- (17) Robinson, I. K.; Bennett, P. A.; Himpfel, F. J. *Phys. Rev. Lett.* **2002**, *88*, 096104.
- (18) Sanchez-Portal, D.; Gale, J. D.; Garcia, A.; Martin, R. M. *Phys. Rev. B* **2002**, *65*, 081401.
- (19) Erwin, S. C. *Phys. Rev. Lett.* **2003**, *91*, 206101.
- (20) Crain, J. N.; Altmann, K. N.; Bromberger, C.; Erwin, S. C.; Kirakosian, A.; McChesney, J. L.; Lin, J.-L.; Himpfel, F. J. *Phys. Rev. Lett.* **2003**, *90*, 176805.
- (21) Crain, J. N.; McChesney, J. L.; Fan Zheng; Gallagher, M.; Snijders, P. C.; Bissen, M.; Gundelach, C.; Erwin, S. C.; Himpfel, F. J. *Phys. Rev. B* **2004**, *69*, 125409.
- (22) Kirakosian, A.; McChesney, J. L.; Bennewitz, R.; Crain, J. N.; Lin, J.-L.; Himpfel, F. J. *Surf. Sci.* **2002**, *498*, L109.
- (23) Bennewitz, R.; Crain, J. N.; Kirakosian, A.; Lin, J.-L.; McChesney, J. L.; Petrovykh, D. Y.; Himpfel, F. J. *Nanotechnology* **2002**, *13*, 499.
- (24) Kirakosian, A.; Bennewitz, R.; Himpfel, F. J.; Bruch, L. W. *Phys. Rev. B* **2003**, *67*, 205412.
- (25) Sun, S.; Murray, C. B.; Weller, D.; Folks, L.; Moser, A. *Science* **2000**, *287*, 1989.
- (26) Pérez-Dieste, V.; Castellini, O. M.; Crain, J. N.; Eriksson, M. A.; Kirakosian, A.; Lin, J.-L.; McChesney, J. L.; Himpfel, F. J. *Appl. Phys. Lett.* **2003**, *83*, 5053.
- (27) Kasemo, B. *Surf. Sci.* **2002**, *500*, 656.
- (28) Cornell, B. A.; Braach-Maksvytis, V. L. B.; King, L. G.; Osman, P. D. J.; Raguse, B.; Wiczorek, L.; Pace, R. J. *Nature* **1997**, *387*, 580.
- (29) Urquhart, S. G.; Ade, H. J. *Phys. Chem. B* **2002**, *106*, 8531.
- (30) Peters, R. D.; Nealey, P. F.; Crain, J. N.; Himpfel, F. J. *Langmuir* **2002**, *18*, 1250.
- (31) Luk, Y.-Y.; Abbott, N. L.; Crain, J. N.; Himpfel, F. J. *J. Chem. Phys.* **2004**, in press.
- (32) Crain, J. N.; Kirakosian, A.; Lin, J.-L.; Gu, Y.; Shah, R. R.; Abbott, N. L.; Himpfel, F. J. *J. Appl. Phys.* **2001**, *90*, 3291.
- (33) Petrovykh, D. Y.; Kimura-Suda, H.; Opdahl, A.; Perez Dieste, V.; Himpfel, F. J.; Tarlov, M. J.; Whitman, L. J. to be published.
- (34) Wu, W.; Lee, I. J.; Chaikin, P. M. *Phys. Rev. Lett.* **2003**, *91*, 056601.
- (35) Crain, J. N.; Altmann, K. N.; Bromberger, C.; Himpfel, F. J. *Phys. Rev. B* **2002**, *66*, 205302.
- (36) Clarke, L. I.; Horinek, D.; Kottas, G. S.; Varaska, N.; Magnera, T. F.; Hinderer, T. P.; Horansky, R.; Michl, J.; Price, J. C. *Nanotechnology* **2002**, *13*, 533.
- (37) Mayne, A. J.; Lastapis, M.; Baffou, G.; Soukiassian, L.; Comtet, G.; Hellner, L.; Dujardin, G. *Phys. Rev. B* **2004**, *69*, 045409.
- (38) Schwartz, M. P.; Halter, R. J.; McMahon, R. J.; Hamers, R. J. J. *Phys. Chem. B* **2003**, *107*, 224.
- (39) Weidkamp, K. P.; Hacker, C. A.; Schwartz, M. P.; Cao, X.; Tromp, R. M.; Hamers, R. J. J. *Phys. Chem. B* **2003**, *107*, 1114.
- (40) Bischler, U.; Bertel, E. *Phys. Rev. Lett.* **1993**, *71*, 2296.
- (41) Bertel, E.; Lehmann, L. *Phys. Rev. Lett.* **1998**, *80*, 1497.
- (42) Hildebrand, M.; Ipsen, M.; Mikhailov, A. S.; Ertl, G. *New J. Phys.* **2003**, *5*, 61.